ISSN 1674-1056
http://cpb.iphy.ac.cn
http://iopscience.iop.org/cpb
中国物理 B
Chinese Physics
中国物理
Chinese Physics B

Shortcut-based quantum gates on superconducting qubits in circuit QED

Zheng-Yin Zhao(赵正印), Run-Ying Yan(闫润瑛), and Zhi-Bo Feng(冯志波)
Citation: Chin. Phys. B, 2021, 30 (**8**): 088501. DOI: 10.1088/1674-1056/abea96
Journal homepage: http://cpb.iphy.ac.cn; http://iopscience.iop.org/cpb

What follows is a list of articles you may be interested in

Manipulation of superconducting qubit with direct digital synthesis

Zhi-Yuan Li(李志远), Hai-Feng Yu(于海峰), Xin-Sheng Tan(谭新生), Shi-Ping Zhao(赵士平), Yang Yu(于扬)
Chin. Phys. B, 2019, 28 (**9**): 098505. DOI: 10.1088/1674-1056/ab37f9

Characterization of barrier-tunable radio-frequency-SQUID for Maxwell's demon experiment

Gang Li(李刚), Suman Dhamala, Hao Li(李浩), Jian-She Liu(刘建设), Wei Chen(陈炜)
Chin. Phys. B, 2018, 27 (**6**): 068501. DOI: 10.1088/1674-1056/27/6/068501

Bridge-free fabrication process for Al/AlO_x/Al Josephson junctions

Ke Zhang(张珂), Meng-Meng Li(李蒙蒙), Qiang Liu(刘强), Hai-Feng Yu(于海峰), Yang Yu(于扬)
Chin. Phys. B, 2017, 26 (**7**): 078501. DOI: 10.1088/1674-1056/26/7/078501

Fabrication of Al/AlO_x/Al junctions using pre-exposure technique at 30-keV e-beam voltage

Dong Lan(兰栋), Guangming Xue(薛光明), Qiang Liu(刘强), Xinsheng Tan(谭新生), Haifeng Yu(于海峰), Yang Yu(于扬)
Chin. Phys. B, 2016, 25 (**8**): 088501. DOI: 10.1088/1674-1056/25/8/088501

Increasing energy relaxation time of superconducting qubits with nonmagnetic infrared filter and shield

Yuhao Liu(刘宇浩), Mengmeng Li(李蒙蒙), Dong Lan(兰栋), Guangming Xue(薛光明), Xinsheng Tan(谭新生), Haifeng Yu(于海峰), Yang Yu(于扬)
Chin. Phys. B, 2016, 25 (**5**): 058501. DOI: 10.1088/1674-1056/25/5/058501

Shortcut-based quantum gates on superconducting qubits in circuit QED*

Zheng-Yin Zhao(赵正印), Run-Ying Yan(闫润瑛), and Zhi-Bo Feng(冯志波)†

School of Science, Xuchang University, Xuchang 461000, *China*

(Received 6 January 2021; revised manuscript received 29 January 2021; accepted manuscript online 1 March 2021)

Construction of optimal gate operations is significant for quantum computation. Here an efficient scheme is proposed for performing shortcut-based quantum gates on superconducting qubits in circuit quantum electrodynamics (QED). Two four-level artificial atoms of Cooper-pair box circuits, having sufficient level anharmonicity, are placed in a common quantized field of circuit QED and are driven by individual classical microwaves. Without the effect of cross resonance, one-qubit NOT gate and phase gate in a decoupled atom can be implemented using the invariant-based shortcuts to adiabaticity. With the assistance of cavity bus, a one-step SWAP gate can be obtained within a composite qubit-photon-qubit system by inversely engineering the classical drivings. We further consider the gate realizations by adjusting the microwave fields. With the accessible decoherence rates, the shortcut-based gates have high fidelities. The present strategy could offer a promising route towards fast and robust quantum computation with superconducting circuits experimentally.

Keywords: superconducting qubit, circuit QED, quantum gate, shortcuts to adiabaticity

PACS: 85.25.–j, 42.50.Pq, 03.67.Lx, 32.80.Xx **DOI:** 10.1088/1674-1056/abea96

1. Introduction

Based on quantum state encoding and superposition principle, quantum computers possess some incomparable advantages to implement some computation tasks when compared with the classical counterparts, and then the research field of quantum computing has attracted tremendous attention in the past two decades.[1–5] According to quantum circuit model, computation execution depends on logic gate operations. By means of a set of universal gates, including two noncommutable one-qubit gates and a controlled two-qubit gate, one can accomplish general computation tasks. Physically, qubits carried by quantum systems are inevitably coupled to the degrees of freedom associated with noisy environment, giving rise to qubit decoherence generally.[6] The decoherence effects induce the fidelity loss especially for multi-qubit gates. To fight against the detrimental decoherence effects, one can improve the intrinsic property and then prolong the system coherence time. Alternatively, considerable efforts have been devoted to exploring some fault-tolerant ways to suppress noise effects.[7–12]

Behaving as artificial atoms, superconducting quantum circuits composed of Josephson junctions hold discrete energy levels, which can be encoded to qubits for performing quantum computation.[13–17] Due to flexible controllability and potential scalability, superconducting qubits have been one of the most promising candidates to quantum information processing.[18–23] Particularly, superconducting artificial atoms can be strongly or ultrastrongly coupled to the quantized cavity field generated by the transmission-line resonator (TLR), which thus forms an excellent device of circuit QED in the microwave range.[24–26] In recent years, by combining the quantized cavity field and classical microwave drivings, the investigation of quantum computation with superconducting circuit QED has made remarkable progress.[27–33] However, compared with natural atoms, superconducting solid-state circuits are easily affected by the decoherence effects caused by environmental noises and control varialbe imperfections.[34,35] Some novel strategies have been put forward for constructing robust quantum gates on superconducting qubits.[36–43]

Stimulated Raman adiabatic passage,[44,45] as one of the powerful approaches, is insensitive to the control parameter fluctuations and timing errors, and it has been adopted to perform coherent operations on superconducting quantum circuits.[46–48] Acting as a typical shortcoming, the relatively long duration times are required by the adiabatic operations. During the recent years, a set of techniques named as shortcuts to adiabaticity (STA),[49–51] generally including invariant-based inverse engineering, counterdiabatic driving, and fast-forward approach, has been developed theoretically and demonstrated experimentally. The methods of STA not only remain the robustness advantage of adiabatic manipulations, but also perform quantum operations within shorter times in the absence of adiabatic requirement. Considering the distinctive features, the STA-based coherent controls have been increasingly applied to exploit fast and robust quantum operations on superconducting artificial atoms.[52–61] In the research subject of quantum information processing, the exploration of optimal and feasible superconducting quantum gates

*Project supported by the Natural Science Foundation of Henan Province, China (Grant No. 212300410388) and the "316" Project Plan of Xuchang University.

†Corresponding author. E-mail: zbfeng010@163.com

© 2021 Chinese Physical Society and IOP Publishing Ltd

is still an interesting issue.

In this paper, we present a theoretical scheme for fast implementing quantum gates on superconducting qubits inside circuit QED in a shortcut manner. Two four-level artificial atoms of Cooper-pair box (CPB) circuits in the charge-phase regime are situated in a common quantized cavity and are individually driven by classical microwaves. By virtue of the invariant-based STA, we perform a NOT gate and a π-phase gate on a single qubit. In the two-photon resonance with large detunings, a composite qubit-photon-qubit system can be obtained effectively, in which a one-step implementation of two-qubit SWAP gate can be realized by inversely engineering the classical drivings. We consider the gate realizations by adjusting the microwave fields of ac voltages and time-dependent fluxes. It is found that these gates are robust by numerically simulating the decoherence effects. The proposed strategy could pave a versatile avenue towards optimized quantum computation with superconducting qubits in circuit QED.

This paper is organized as follows. Section 2 presents two four-level artificial atoms of CPBs in a circuit QED. By the technique of invariant-based STA, two one-qubit gates within a decoupled atom and a two-qubit SWAP gate in a composite system are elaborated in Section 3. Section 4 concerns the gate implementations and fidelities. Discussion and a conclusion are finally drawn in Section 5.

2. Two artificial atoms of CPBs in a circuit QED

As schematically depicted in Fig. 1(a), we deal with a high-quality coplanar circuit QED architecture, in which the resonator of length $L_{\rm r}$ along the x direction generates a quantized cavity field with a single-mode frequency $\omega_{\rm r}$. Two CPB circuits are connected to a one-dimensional resonator via capacitances $C_{\rm r}^{(k)}$ (with $k=1$ and 2), leading to electrical interactions between the CPBs and quantized field. Each CPB circuit contains a box with extra Cooper-pairs n. The box is linked to a segment of a superconducting loop via two identical Josephson junctions with coupling energies $E_{\rm J}$ and capacitances $C_{\rm J}$. The total Josephson energy $\bar{E}_{\rm J}^{(k)}$ can be adjusted by means of a magnetic flux $\Phi_{\rm s}^{(k)}$ threading the loop. Through a gate capacitance $C_{\rm g}$, a static bias voltage $V_{\rm g}^{(k)}$ is applied to the kth box. Apart from the static voltage $V_{\rm g}^{(k)}$ and flux $\Phi_{\rm s}^{(k)}$, an ac voltage $\tilde{V}_d^{(k)}$ and time-dependent flux $\tilde{\Phi}_m^{(k)}$, acting as classical microwave drivings, exert on the kth CPB to induce level state transitions, as mentioned later.

In the charge-phase regime,[62] the characteristic system parameters fulfill $E_{\rm c}^{(k)} \sim \bar{E}_{\rm J}^{(k)}$, where $E_{\rm c}^{(k)}$ is the charging energy scale with the same order of $\bar{E}_{\rm J}^{(k)}$. With no radiations from the quantized and classical fields, the system Hamiltonian of a single CPB is

$$H_0^{(k)} = E_{\rm c}^{(k)}[n-n_{\rm g}^{(k)}]^2 - \bar{E}_{\rm J}^{(k)}\cos\theta, \tag{1}$$

where the first and second terms represent the system charging and Josephson energies, respectively. We have $E_{\rm c}^{(k)} = 2e^2/C_{\rm t}^{(k)}$, with $C_{\rm t}^{(k)} = (C_{\rm g}+C_{\rm d}^{(k)}+C_{\rm r}^{(k)}+2C_{\rm J})$ being the total capacitance of the box, and $n_{\rm g}^{(k)} = C_{\rm g}V_{\rm g}^{(k)}/2e$ indicates the offset charge. The total Josephson energy reads $\bar{E}_{\rm J}^{(k)} = 2E_{\rm J}\cos[\pi\Phi_{\rm s}^{(k)}/\Phi_0]$, with $\Phi_0 = h/2e$ being the flux quantum. As an average phase difference of the two junctions, θ is canonically conjugate to n, namely, $[\theta, n] = i$.

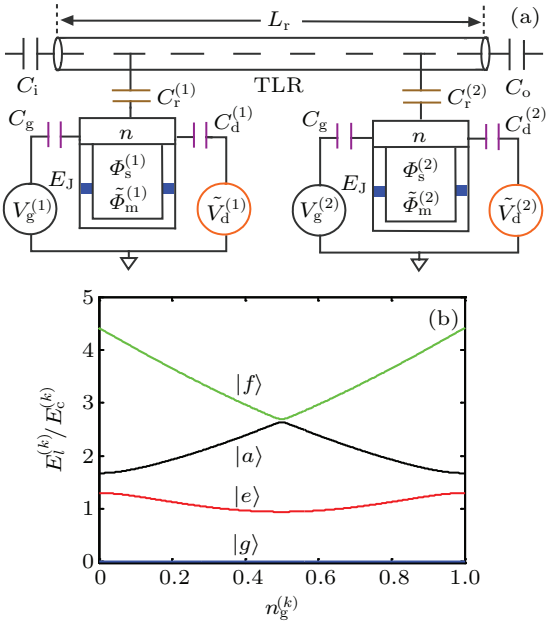


Fig. 1. (a) Schematic demonstration of two CPBs connected to a one-dimensional TLR, the kth CPB is driven by the controllable classical microwaves $\tilde{V}_{\rm d}^{(k)}$ and $\tilde{\Phi}_m^{(k)}$, with $k=1$ and 2. (b) The first four levels $E_l^{(k)}$ of the kth CPB (with $\bar{E}_{\rm J}^{(k)} = E_{\rm c}^{(k)}$) versus gate charge $n_{\rm g}^{(k)}$, with $l =$ g, e, a, and f. Here the energies are given in units of $E_{\rm c}^{(k)}$, and $E_{\rm g}^{(k)}$ has been taken as the zero-energy references.

In terms of Eq. (1), the $n_{\rm g}^{(k)}$-dependent eigenlevels and eigenstates of the kth CPB circuit can be obtained. We have the first four levels $E_l^{(k)}$ (with $l =$ g, e, a, and f) versus $n_{\rm g}^{(k)}$, as given in Fig. 1(b). The CPB system with discrete levels is often referred to as artificial atom. The eigenstates $|l\rangle$ can be expressed as superpositions of Cooper-pair number states, $|l\rangle = \sum_n c_{ln}|n\rangle$, with c_{ln} being combination coefficients. At a bias point $n_{\rm g}^{(k)} = 0.4$, the level states $|l\rangle$ constitute an effective four-level system, which has a sufficiently large level anharmonicity. In this case, the transition frequencies $\omega_{\rm ae}^{(k)} = [E_{\rm a}^{(k)} - E_{\rm e}^{(k)}]/\hbar$ and $\omega_{\rm eg}^{(k)} = [E_{\rm e}^{(k)} - E_{\rm g}^{(k)}]/\hbar$ are far away from each other, which is highly beneficial to eliminate leakage errors.

With the chosen $E_{\rm c}^{(1)}$ and $E_{\rm c}^{(2)}$, there exist obvious frequency differences $\omega_{\rm ae}^{(2)} - \omega_{\rm ae}^{(1)}$ and $\omega_{\rm eg}^{(2)} - \omega_{\rm eg}^{(1)}$ between two atoms in our scenario. Since the eigenstates $|l\rangle^{(1)}$ and $|l\rangle^{(2)}$ are identical correspondingly, the superscripts of $|l\rangle^{(k)}$ in Fig. 1(b) have been ignored. Here, $|g\rangle^{(k)}$ and $|e\rangle^{(k)}$ are encoded into qubit states, while $|a\rangle^{(k)}$ and $|f\rangle^{(k)}$ serve as ancillary states. The current choice of $n_{\rm g}^{(k)} = 0.4$ is based on a balance of

two aspects. On the one hand, qubit states at a magic point ($n_g = 0.5$) can be well immune to the first-order fluctuation of gate charge,[62] contributing to prolong the qubit coherence time. Thereby, to keep the advantage as much as possible, the bias point should be close to $n_g = 0.5$. On the other hand, the working points should be appropriately deviated from 0.5 for obtaining sufficient level separations between $|a\rangle^{(k)}$ and $|f\rangle^{(k)}$.

3. STA-based quantum gates

3.1. Two one-qubit gates

Before constructing one-qubit gates, two CPBs in a cavity field need to be decoupled from each other. The cavity mode of frequency ω_r aims at causing the couplings between $|e\rangle^{(k)}$ and $|a\rangle^{(k)}$, the coupling strengths of which are assumed to be $\lambda^{(1)}$ and $\lambda^{(2)}$, see Fig. 2(a). Since the cavity frequency ω_r is largely detuned from the transition frequencies $\omega_{ae}^{(k)}$, we have the detunings $\Delta^{(k)} = \omega_{ae}^{(k)} - \omega_r$ much larger than $\lambda^{(k)}$. When the difference $\Delta^{(21)} = \Delta^{(2)} - \Delta^{(1)}$ is large enough, the cross resonance between $|e\rangle^{(1)}|a\rangle^{(2)}$ and $|a\rangle^{(1)}|e\rangle^{(2)}$ that is induced by the cavity field can be suppressed effectively.[63,64] Moreover, in the dispersive regime, the cavity field cannot directly trigger the transition between $|e\rangle^{(k)}$ and $|a\rangle^{(k)}$ within each atom. In this situation, two atoms will not be affected by the cavity field,[65] and then we can individually address each atom.

First, we start with a one-qubit NOT gate within a decoupled atom, for example, the 1st atom. As shown in Fig. 2(b), within a subspace $\{|g\rangle, |a\rangle, |e\rangle\}^{(1)}$, two classical microwave drivings with resonant frequencies result in a Λ-configuration interaction with Rabi couplings $\Omega_{ag}^{(1)}$ and $\Omega_{ae}^{(1)}$. The interaction Hamiltonian is described by

$$H_n(t) = \hbar[\Omega_{ag}^{(1)}|a\rangle\langle g| + \Omega_{ae}^{(1)}|a\rangle\langle e| + \text{H.c.}]. \tag{2}$$

The invariant of Hamiltonian in Eq. (2) reads

$$\begin{aligned} I_n(t) =\ & \hbar\Omega_n(\cos\alpha\sin\beta|a\rangle\langle g| + \cos\alpha\cos\beta|a\rangle\langle e| \\ & + \mathrm{i}\sin\alpha|e\rangle\langle g| + \text{H.c.}), \end{aligned} \tag{3}$$

where Ω_n is a constant in units of frequency to keep $I_n(t)$ with dimensions of energy. The three eigenstates of $I_n(t)$ are derived as

$$\begin{aligned} |\phi_0(t)\rangle =\ & \cos\alpha\cos\beta|g\rangle - \mathrm{i}\sin\alpha|a\rangle - \cos\alpha\sin\beta|e\rangle, \\ |\phi_\pm(t)\rangle =\ & \frac{1}{\sqrt{2}}[(\sin\alpha\cos\beta \pm \mathrm{i}\sin\beta)|g\rangle + \mathrm{i}\cos\alpha|a\rangle \\ & -(\sin\alpha\sin\beta \mp \mathrm{i}\cos\beta)|e\rangle], \end{aligned}$$

the eigenvalues of which are $\lambda_0 = 0$ and $\lambda_\pm = \pm\Omega_n$, respectively. The relations between the Rabi couplings and the parameters α and β satisfy

$$\begin{aligned} \Omega_{ag}^{(1)} =\ & \dot\beta\cot\alpha\sin\beta + \dot\alpha\cos\beta, \\ \Omega_{ae}^{(1)} =\ & \dot\beta\cot\alpha\cos\beta - \dot\alpha\sin\beta. \end{aligned}$$

The time evolution of an arbitrary state $|\psi(t)\rangle$ obeys the Schrödinger equation, $\mathrm{i}\hbar\frac{\mathrm{d}}{\mathrm{d}t}|\psi(t)\rangle = H_n(t)|\psi(t)\rangle$, in which $|\psi(t)\rangle$ can be expressed as a superposition of $|\phi_0(t)\rangle$ and $|\phi_\pm(t)\rangle$, namely,

$$|\psi(t)\rangle = \sum_{m=0,\pm} C_m \mathrm{e}^{\mathrm{i}\gamma_m(t)}|\phi_m(t)\rangle,$$

where C_m are time-independent probability amplitudes, and

$$\gamma_m(t) = \frac{1}{\hbar}\int_0^t \mathrm{d}t' \langle\phi_m(t')|\,\mathrm{i}\hbar\frac{\partial}{\partial t'} - H_n(t')\,|\phi_m(t')\rangle$$

are Lewis–Riesenfeld phases.[66]

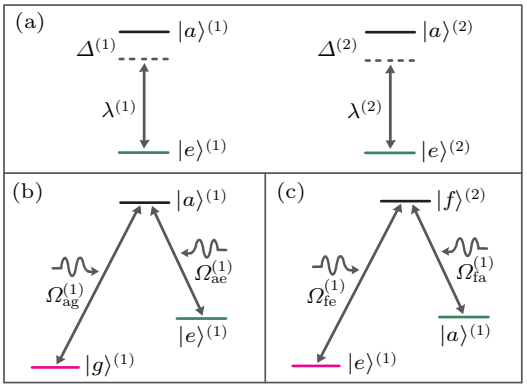


Fig. 2. (a) The cavity-induced Rabi couplings $\lambda^{(k)}$ between $|e\rangle^{(k)}$ and $|a\rangle^{(k)}$, and large detunings $\Delta^{(k)}$ exist between $\omega_{ae}^{(k)}$ and ω_r, with $k = 1$ and 2. (b) Within a subspace $\{|g\rangle, |a\rangle, |e\rangle\}^{(1)}$ of the 1st CPB, there is a Λ-configuration interaction with Rabi coupling $\Omega_{ag}^{(1)}$ ($\Omega_{ae}^{(1)}$) between $|a\rangle$ and $|g\rangle$ ($|e\rangle$). (c) Within a subspace $\{|e\rangle, |f\rangle, |a\rangle\}^{(1)}$, Rabi coupling $\Omega_{fe}^{(1)}$ ($\Omega_{fa}^{(1)}$) between $|f\rangle$ and $|e\rangle$ ($|a\rangle$) occurs in the 1st CPB.

We parameterize α and β as functions of time $t \in [0, t_n]$,

$$\alpha = \varepsilon, \quad \beta = \frac{3\pi}{2t_n}t, \tag{4}$$

where t_n is a final time, ε is a constant. At the initial time $t = 0$, the eigenstates $|\phi_m\rangle$ are

$$\begin{aligned} |\phi_0(0)\rangle =\ & \cos\varepsilon|g\rangle - \mathrm{i}\sin\varepsilon|a\rangle, \\ |\phi_\pm(0)\rangle =\ & \frac{1}{\sqrt{2}}[\sin\varepsilon|g\rangle + \mathrm{i}\cos\varepsilon|a\rangle \pm \mathrm{i}|e\rangle]. \end{aligned}$$

Differently, the eigenstates at the final time $t = t_n$ change to

$$\begin{aligned} |\phi_0(t_n)\rangle =\ & -\mathrm{i}\sin\varepsilon|a\rangle + \cos\varepsilon|e\rangle, \\ |\phi_\pm(t_n)\rangle =\ & \frac{1}{\sqrt{2}}(\mp\mathrm{i}|g\rangle + \mathrm{i}\cos\varepsilon|a\rangle + \sin\varepsilon|e\rangle). \end{aligned}$$

Assume that the system state is initially in $|\psi(0)\rangle = c_g|g\rangle + c_e|e\rangle$, with $c_{g,e}$ being superposition coefficients, we obtain $C_0 = c_g\cos\varepsilon$ and $C_\pm = (c_g\sin\varepsilon \pm \mathrm{i}c_e)/\sqrt{2}$. After a coherent evolution driven by the present pulses $\Omega_{ag}^{(1)}$ and $\Omega_{ae}^{(1)}$, the final state yields $|\psi(t_n)\rangle = \sum_{m=0,\pm} C_m \mathrm{e}^{\mathrm{i}\gamma_m(t_n)}|\phi_m(t_n)\rangle$, where the phases take $\gamma_0(t_n) = 0$ and

$$\gamma_\pm(t_n) = \mp\int_0^{t_n}[\dot\beta\sin\varepsilon + (\Omega_{ag}^{(1)}\sin\beta + \Omega_{ae}^{(1)}\cos\beta)\cos\varepsilon]\,\mathrm{d}t.$$

In this case, we have the following state

$$\begin{aligned}|\psi(t_n)\rangle \;=\; & (-c_{\rm g}\sin\varepsilon\sin\gamma+c_{\rm e}\cos\gamma)\,|g\rangle+\\ & (-{\rm i}c_{\rm g}\sin\varepsilon\cos\varepsilon+{\rm i}c_{\rm g}\cos\varepsilon\sin\varepsilon\cos\gamma\\ & +{\rm i}c_{\rm e}\cos\varepsilon\sin\gamma)\,|a\rangle+(c_{\rm g}\cos^2\varepsilon+\\ & c_{\rm g}\sin^2\varepsilon\cos\gamma+c_{\rm e}\sin\varepsilon\sin\gamma)\,|e\rangle\,, \end{aligned}\tag{5}$$

in which $\gamma(=|\gamma_{\pm}(t_n)|)=3\pi/(2\sin\varepsilon)$. When $\gamma=2N\pi$ (with $N=1,2,3,\ldots$), the final state becomes

$$|\psi(t_n)\rangle = c_{\rm e}\,|g\rangle+c_{\rm g}\,|e\rangle\,.$$

Apparently, no population of $|a\rangle$ occurs at the initial and final times. Within the qubit state basis, an initial input state $|\psi_{\rm in}\rangle=c_{\rm g}\,|g\rangle+c_{\rm e}\,|e\rangle$ will evolve into an output state $|\psi_{\rm out}\rangle=c_{\rm e}\,|g\rangle+c_{\rm g}\,|e\rangle$ after a duration time $t=t_n$. In the framework of quantum computing, such a process is just a NOT-gate operation on the encoded qubit.

Secondly, we address a π-phase gate operation on the 1st qubit. At the initial time $t=0$, an input qubit state is expressed as $|\psi_{\rm in}\rangle=c_{\rm g}\,|g\rangle+c_{\rm e}\,|e\rangle$. At a final time $t=t_{\rm p}$, the output state needs to be $|\psi_{\rm out}\rangle=c_{\rm g}\,|g\rangle-c_{\rm e}\,|e\rangle$, which has a π-phase accumulation on $|e\rangle$. To this end, we consider a coherent operation within another subspace $\{|e\rangle,|f\rangle,|a\rangle\}^{(1)}$. By tuning the microwave frequency $\omega_m^{(1)}$ ($\omega_{\rm d}^{(1)}$) of driving field $\tilde{\Phi}_m^{(1)}$ ($\tilde{V}_{\rm d}^{(1)}$), we obtain $\omega_m^{(1)}=\omega_{\rm fe}^{(1)}$ and $\omega_{\rm d}^{(1)}=\omega_{\rm fa}^{(1)}$, respectively. By adopting the resonant drivings, the transitions between $|f\rangle$ and $|e\rangle$ ($|a\rangle$) with Rabi couplings $\Omega_{\rm fe}^{(1)}$ ($\Omega_{\rm fa}^{(1)}$) appear within the subspace having a large level anharmonicity as well. In the two-photon resonance, as displayed in Fig. 2(c), the interaction Hamiltonian is given by

$$H_{\rm p}(t)=\hbar[\Omega_{\rm fe}^{(1)}\,|f\rangle\langle e|+\Omega_{\rm fa}^{(1)}\,|f\rangle\langle a|+{\rm H.c.}],\tag{6}$$

which has a dynamical symmetry same as that of $H_n(t)$. Thereby, the invariant $I_{\rm p}(t)$ of $H_{\rm p}(t)$ is similar to $I_n(t)$ in Eq. (3).

To implement the π-phase operation on state $|e\rangle$, as mentioned in Ref. [67], the dependencies of parameters α and β on time $t\in[0,t_{\rm p}]$ meet

$$\alpha=\varepsilon,\quad \beta=\frac{\pi}{t_{\rm p}}t,\tag{7}$$

which determine the initial and final eigenstates of $I_{\rm p}(t)$. Meanwhile, the time-dependent Rabi couplings take

$$\begin{aligned}\Omega_{\rm fe}^{(1)} &= \frac{\pi}{t_{\rm p}}\cot\varepsilon\sin\left(\frac{\pi}{t_{\rm p}}t\right),\\ \Omega_{\rm fa}^{(1)} &= \frac{\pi}{t_{\rm p}}\cot\varepsilon\cos\left(\frac{\pi}{t_{\rm p}}t\right).\end{aligned}$$

For an initial system state $|\psi(0)\rangle=|e\rangle$, there are $C_0=\cos\varepsilon$ and $C_{\pm}=\frac{1}{\sqrt{2}}\sin\varepsilon$. After an evolution time $t=t_{\rm p}$, the final system state is

$$\begin{aligned}\big|\psi(t_{\rm p})\big\rangle \;=\; & -(\cos^2\varepsilon+\sin^2\varepsilon\cos\gamma)\,|e\rangle+({\rm i}\sin\varepsilon\cos\varepsilon\cos\gamma\\ & -{\rm i}\cos\varepsilon\sin\varepsilon)\,|f\rangle-\sin\varepsilon\sin\gamma|a\rangle\,.\end{aligned}\tag{8}$$

When the phase factor is $\gamma(=\pi/\sin\varepsilon)=2N\pi$ (with $N=1,2,3,\ldots$), the final state becomes $\big|\psi(t_{\rm p})\big\rangle=-|e\rangle$. Since the qubit state $|g\rangle$ is not involved during the whole evolution, the input state $|\psi_{\rm in}\rangle=c_{\rm g}\,|g\rangle+c_{\rm e}\,|e\rangle$ will change to $|\psi_{\rm out}\rangle=c_{\rm g}\,|g\rangle-c_{\rm e}\,|e\rangle$ in the operation time $t=t_{\rm p}$, enabling a π-phase accumulation on qubit state $|e\rangle$. As a result, we obtain a π-phase gate by the invariant-based shortcut.

3.2. Two-qubit SWAP gate

To perform a two-qubit SWAP gate, we first focus on the effective interaction between two qubits. As displayed in Fig. 3(a), through the creation (annihilation) of cavity photon, the quantized field induces couplings between $|e\rangle^{(k)}$ and $|a\rangle^{(k)}$ with Rabi frequencies $\lambda^{(k)}$. The couplings $\Omega_{\rm ag}^{(k)}$ between $|a\rangle^{(k)}$ and $|g\rangle^{(k)}$ can be realized by applying two individual drivings $\tilde{\Phi}_m^{(k)}$, with $k=1,2$. In our scenario, $\lambda^{(k)}$ are constants while $\Omega_{\rm ag}^{(k)}$ are adjustable. In the two-photon resonance with detunings $\Delta^{(k)}$, there exists $\omega_{\rm ae}^{(k)}-\omega_{\rm r}=\omega_{\rm ag}^{(k)}-\omega_m^{(k)}=\Delta^{(k)}$, and two Λ-configuration interactions occur within the atoms.

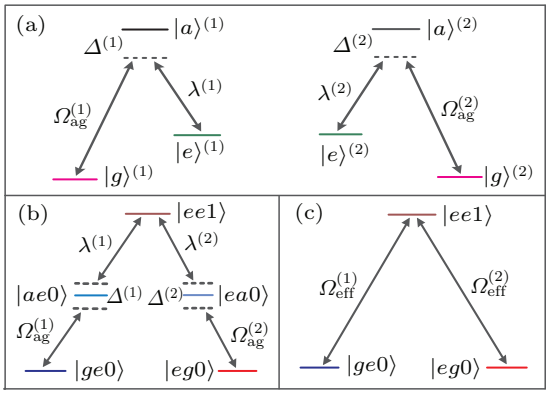


Fig. 3. (a) In the two-photon resonances $\omega_{\rm ag}^{(k)}-\omega_m=\omega_{\rm ae}^{(k)}-\omega_{\rm r}=\Delta^{(k)}$, cavity field couples states $|a\rangle^{(k)}$ to $|e\rangle^{(k)}$ (with $k=1,2$), two individual pulses $\Omega_{\rm ag}^{(k)}$ lead to couplings of $|g\rangle^{(k)}$ to $|a\rangle^{(k)}$. (b) Within the composite state space $\{|ge0\rangle,|ae0\rangle,|ee1\rangle,|ea0\rangle,|eg0\rangle\}$, the interactions of qutrits 1 and 2 with external fields. (c) For the large detunings $\Delta^{(k)}$, a reduced composite system $\{|ge0\rangle,|ee1\rangle,|eg0\rangle\}$ with effective Rabi couplings $\Omega_{\rm eff}^{(k)}$.

To explicitly illustrate the cavity-mediated interaction between two atoms, we consider the state couplings within a composite system $\{|ge0\rangle,|ae0\rangle,|ee1\rangle,|ea0\rangle,|eg0\rangle\}$, where the symbols in each product state represent the quantum states of atoms 1, 2, and cavity photon, respectively. For simplicity, the superscripts of product states have been omitted here. In the composite system, the interaction only associated with atom 1, as sketched on the left side of Fig. 3(b), gives rise to a coupling of $|g\rangle^{(1)}|0\rangle$ to $|e\rangle^{(1)}|1\rangle$ via an intermediate state $|a\rangle^{(1)}|0\rangle$. Within the atom 2, the coupling between $|e\rangle^{(2)}|1\rangle$ and $|g\rangle^{(2)}|0\rangle$ can be built with the assistance of $|a\rangle^{(2)}|0\rangle$, see the right side of Fig. 3(b). In this situation, the cavity field plays a role of data bus to couple target states $|ge\rangle$ and $|eg\rangle$.

In the regime of large detunings $\Delta^{(k)} \gg \Omega_{\rm ag}^{(k)}$ and $\lambda^{(k)}$, the intermediate states $|a\rangle^{(k)}$ are not populated almost. After adiabatically removing $|a\rangle^{(k)}$, these two qutrits can be reduced to two-level systems only containing $|e\rangle^{(k)}$ and $|g\rangle^{(k)}$.[68] Based on an auxiliary state $|ee1\rangle$, the transitions $|ge0\rangle \leftrightarrow |ee1\rangle$ and $|ee1\rangle \leftrightarrow |ge0\rangle$ cause a resulting coupling between $|ge0\rangle$ and $|eg0\rangle$, as depicted in Fig. 3(c). The effective Rabi couplings are given by

$$\Omega_{\rm eff}^{(k)} = -\frac{\lambda^{(k)}\Omega_{\rm ag}^{(k)}}{2\Delta^{(k)}}. \tag{9}$$

Then the indirect coupling between two qubits can be realized in this way. For the fixed $\lambda^{(k)}$ and $\Delta^{(k)}$, it is found that $\Omega_{\rm eff}^{(k)}$ can be adjusted by the variables $\Omega_{\rm ag}^{(k)}$. Within a reduced subspace $\{|ge0\rangle, |ee1\rangle, |eg0\rangle\}$ of interest, we can perform coherent operations by the manipulations of $\Omega_{\rm eff}^{(1)}$ and $\Omega_{\rm eff}^{(2)}$ following the central idea of STA.

Next, we deal with the construction of two-qubit SWAP gate. The Hamiltonian describing an effective interaction as given in Fig. 3(c) is

$$H_{\rm s} = \hbar[\Omega_{\rm eff}^{(1)}|ge0\rangle\langle ee1| + \Omega_{\rm eff}^{(2)}|eg0\rangle\langle ee1| + {\rm H.c.}]. \tag{10}$$

The invariant $I_{\rm s}$ of $H_{\rm s}$ is as follows:

$$\begin{aligned} I_{\rm s} =\ & \hbar\Omega_{\rm s}(\cos\alpha\sin\beta|ee1\rangle\langle ge0| + \cos\alpha\cos\beta|ee1\rangle\langle eg0| \\ & + {\rm i}\sin\alpha|eg0\rangle\langle ge0| + {\rm H.c.}), \end{aligned} \tag{11}$$

which has three eigenstates,

$$\begin{aligned} |\phi_0(t)\rangle =\ & \cos\alpha\cos\beta|ge0\rangle - {\rm i}\sin\alpha|ee1\rangle - \cos\alpha\sin\beta|eg0\rangle, \\ |\phi_\pm(t)\rangle =\ & \frac{1}{\sqrt{2}}[(\sin\alpha\cos\beta \pm {\rm i}\sin\beta)|ge0\rangle + {\rm i}\cos\alpha|ee1\rangle \\ & -(\sin\alpha\sin\beta \mp {\rm i}\cos\beta)|eg0\rangle]. \end{aligned}$$

An arbitrary state $|\psi(t)\rangle$ of the composite system can be expressed as a superposition of $|\phi_0(t)\rangle$ and $|\phi_\pm(t)\rangle$, namely, $|\psi(t)\rangle = \sum_{m=0,\pm} C_m {\rm e}^{{\rm i}\gamma_m(t)}|\phi_m(t)\rangle$.

To acquire a two-qubit SWAP gate, the parameters α and β are designed as functions of time $t \in [0, t_{\rm s}]$,

$$\alpha(t) = \varepsilon, \quad \beta(t) = \frac{3\pi}{2t_{\rm s}}t, \tag{12}$$

which enable the effective Rabi couplings to be expressed as

$$\begin{aligned} \Omega_{\rm eff}^{(1)} &= \frac{3\pi}{2t_{\rm s}}\cot\varepsilon\sin\left(\frac{3\pi}{2t_{\rm s}}t\right), \\ \Omega_{\rm eff}^{(2)} &= \frac{3\pi}{2t_{\rm s}}\cot\varepsilon\cos\left(\frac{3\pi}{2t_{\rm s}}t\right). \end{aligned}$$

Provided that the system is initially in $|\psi(0)\rangle = c_{\rm ge}|ge0\rangle + c_{\rm eg}|eg0\rangle$, we can reach $C_0 = c_{\rm ge}\cos\varepsilon$ and $C_\pm = (c_{\rm ge}\sin\varepsilon \pm {\rm i}c_{\rm eg})/\sqrt{2}$. After the evolution time $t = t_{\rm s}$, the system state yields

$$\begin{aligned} |\psi(t_{\rm s})\rangle =\ & (-c_{\rm ge}\sin\varepsilon\sin\gamma + c_{\rm eg}\cos\gamma)|ge0\rangle \\ & + (-{\rm i}c_{\rm ge}\sin\varepsilon\cos\varepsilon + ic_{\rm ge}\cos\varepsilon\sin\varepsilon\cos\gamma \\ & + {\rm i}c_{\rm eg}\cos\varepsilon\sin\gamma)|ee1\rangle + (c_{\rm ge}\cos^2\varepsilon \\ & + c_{\rm ge}\sin^2\varepsilon\cos\gamma + c_{\rm eg}\sin\varepsilon\sin\gamma)|eg0\rangle. \end{aligned} \tag{13}$$

When $\gamma = 2N\pi$ (with $N = 1, 2, 3, \ldots$), we have $|\psi(t_{\rm s})\rangle = c_{\rm ge}|eg0\rangle + c_{\rm eg}|ge0\rangle$. For a two-qubit input state $|\psi_{\rm in}\rangle = c_{\rm gg}|gg\rangle + c_{\rm ge}|ge\rangle + c_{\rm eg}|eg\rangle + c_{\rm ee}|ee\rangle$, the output state is then $|\psi_{\rm out}\rangle = c_{\rm gg}|gg\rangle + c_{\rm ge}|eg\rangle + c_{\rm eg}|ge\rangle + c_{\rm ee}|ee\rangle$, since $|gg\rangle$ and $|ee\rangle$ do not take part in the evolution. As a consequence, a two-qubit SWAP gate can be executed within the composite system.

4. Gate implementations and fidelities

In what follows, we concern the required microwave drivings to implement the above mentioned gate operations. First of all, based on the Rabi coupling $\Omega_{\rm ag}^{(1)}$ ($\Omega_{\rm ae}^{(1)}$) that is caused by pulse driving $\tilde{\Phi}_m^{(1)}$ ($\tilde{V}_{\rm d}^{(1)}$), we give the performance of one-qubit NOT gate. The time-dependent flux has a form of $\tilde{\Phi}_m^{(1)} = \Phi_m^{(1)}\cos[\omega_m^{(1)}t]$, where $\Phi_m^{(1)}$ is an adjustable amplitude, the microwave frequency $\omega_m^{(1)}$ is tuned to be in resonance with $\omega_{\rm ag}^{(1)}$. Thus the magnetic coupling between $|a\rangle$ and $|g\rangle$ can be induced by means of the flux driving. With the rotating-wave approximation (RWA), the relevant Rabi coupling is

$$\Omega_{\rm ag}^{(1)} = \frac{E_{\rm J}}{2}\pi\frac{\Phi_m^{(1)}}{\Phi_0}\sin\left[\frac{\pi\Phi_{\rm s}^{(1)}}{\Phi_0}\right]O_{\rm ag}/\hbar, \tag{14}$$

where $O_{\rm ag} \simeq -0.645$ is the state overlap between $|a\rangle$ and $|g\rangle$ at the bias point $n_{\rm g}^{(1)} = 0.4$,[60] the static flux is chosen as $\Phi_{\rm s}^{(1)} = \Phi_0/3$, and the Josephson coupling takes $E_{\rm J}/\hbar = 2\pi \times 8500$ MHz. When the amplitude of bias flux satisfies $\Phi_m^{(1)} \simeq 0.015\Phi_0\sin(\frac{3\pi}{2t_n}t)$, behaving as a function of time $t \in [0, t_n]$, the coupling strength takes $\Omega_{\rm ag}^{(1)}/2\pi \simeq -110.2\sin(\frac{3\pi}{2t_n}t)$ MHz.

With the aid of ac voltage $\tilde{V}_{\rm d}^{(1)} = V_{\rm d}^{(1)}\cos[\omega_{\rm d}^{(1)}t]$, the coupling between $|a\rangle$ and $|e\rangle$ can be obtained, where the time-dependent amplitude $V_{\rm d}^{(1)}$ is controllable, and $\omega_{\rm d}^{(1)}$ is in resonance with $\omega_{\rm ae}^{(1)}$. With the RWA, the Rabi coupling is in the form of

$$\Omega_{\rm ae}^{(1)} = -E_{\rm c}^{(1)}O_{\rm ae}n_{\rm d}^{(1)}/\hbar, \tag{15}$$

where $O_{\rm ae} \simeq 0.291$ is the overlap between $|a\rangle$ and $|e\rangle$, and $n_{\rm d}^{(1)} = C_{\rm d}^{(1)}V_{\rm d}^{(1)}/2e$. By setting the gate voltage $V_{\rm d}^{(1)}$, we have $n_{\rm d}^{(1)} \simeq 0.045\cos(\frac{3\pi}{2t_n}t)$ within a time domain $t \in [0, t_n]$. In this case, the Rabi coupling changes $\Omega_{\rm ae}^{(1)}/2\pi \simeq -110.2\sin(\frac{3\pi}{2t_n}t)$ MHz for $E_{\rm c}^{(1)} = E_{\rm J}$, which has an amplitude as same as that of $\Omega_{\rm ag}^{(1)}/2\pi$.

Based on the designed couplings $\Omega_{\rm ag}^{(1)}$ and $\Omega_{\rm ae}^{(1)}$, we analyze the time evolution of state $|\psi(t)\rangle$ by numerically solving the Schrödinger equation, ${\rm i}\hbar\frac{\rm d}{{\rm d}t}|\psi(t)\rangle = H_n(t)|\psi(t)\rangle$. As an example, an initial state $|g\rangle$ can be coherently transferred to $|e\rangle$ in an operation time $t_n = 6$ ns, see Fig. 4(a). Compared with

Eq. (4), $\varepsilon = a\sin(3/4)$ is taken here. Thereby, an input qubit state $|\psi_{\rm in}\rangle = c_{\rm g}|g\rangle + c_{\rm e}|e\rangle$ is transformed into an output state $|\psi_{\rm out}\rangle = c_{\rm g}|e\rangle + c_{\rm e}|g\rangle$, with $c_{\rm g} = 1$ and $c_{\rm e} = 0$. Consequently, such a process implements a one-qubit NOT operation.

Secondly, we concentrate on the performance of π-phase gate. The employed $\Omega_{\rm fe}^{(1)}$ and $\Omega_{\rm fa}^{(1)}$ can be induced using the adjustable microwave drivings $\tilde{\Phi}_m^{(1)} = \Phi_m^{(1)}\cos[\omega_m^{(1)}t]$ and $\tilde{V}_{\rm d}^{(1)} = V_{\rm d}^{(1)}\cos[\omega_{\rm d}^{(1)}t]$, respectively, in which the frequencies $\omega_m^{(1)}$ and $\omega_{\rm d}^{(1)}$ are tuned to be resonant with $\omega_{\rm fe}^{(1)}$ and $\omega_{\rm fa}^{(1)}$. The Rabi coupling between $|f\rangle$ and $|e\rangle$ caused by the magnetic interaction meets

$$\Omega_{\rm fe}^{(1)} = \frac{E_{\rm J}}{2}\pi\frac{\Phi_m^{(1)}}{\Phi_0}\sin\left[\frac{\pi\Phi_{\rm s}^{(1)}}{\Phi_0}\right]O_{\rm fe}/\hbar, \tag{16}$$

where $O_{\rm fe} \simeq 0.906$ is the state overlap, and the RWA has been adopted. For a flux $\Phi_m^{(1)} \simeq 0.005\Phi_0\sin(\frac{\pi}{t_{\rm p}}t)$, we obtain $\Omega_{\rm fe}^{(1)}/2\pi \simeq 57.7\sin(\frac{\pi}{t_{\rm p}}t)$ MHz. In addition, the electrical interaction-induced Rabi coupling between $|f\rangle$ and $|a\rangle$ is expressed as

$$\Omega_{\rm fa}^{(1)} = -E_{\rm c}^{(1)}O_{\rm fa}n_{\rm d}^{(1)}/\hbar, \tag{17}$$

with $O_{\rm fa} \simeq 0.150$. When $n_{\rm d}^{(1)}$ is chosen as $n_{\rm d}^{(1)} \simeq 0.044\cos(\frac{\pi}{t_{\rm p}}t)$, the Rabi coupling takes $\Omega_{\rm fa}^{(1)}/2\pi \simeq -57.7\cos(\frac{\pi}{t_{\rm p}}t)$ MHz. Based on the designed drivings, quantum state evolution from $|e\rangle$ to $-|e\rangle$ can be achieved by numerically simulating the Schrödinger equation, $i\hbar\frac{\rm d}{{\rm d}t}|\psi(t)\rangle = H_{\rm p}(t)|\psi(t)\rangle$. As displayed in Fig. 4(b), the operation has a duration time $t_{\rm p} = 15$ ns and the corresponding constant is $\varepsilon = \arcsin(1/2)$.

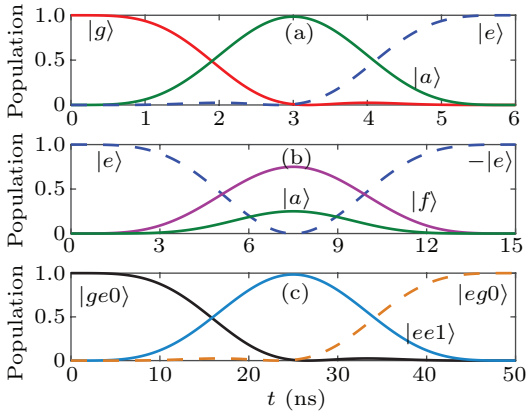


Fig. 4. (a) For a NOT gate operation, an initial state $|g\rangle$ evolves to $|e\rangle$ in a time $t_n = 6$ ns. (b) For the π-phase gate, an initial input state $|e\rangle$ evolves to a final output state $-|e\rangle$ after a duration time $t_{\rm p} = 15$ ns. (c) Within a composite system, a final state $|eg0\rangle$ is obtained from an initial state $|ge0\rangle$ in a time $t_{\rm s} = 50$ ns.

Next, the couplings $\Omega_{\rm eff}^{(1)}$ and $\Omega_{\rm eff}^{(2)}$ for implementing a two-qubit SWAP gate are our concern. The artificial atoms electrically interact with a standing-wave cavity field. A quantized voltage $V_{\rm r}$ generated by the resonator takes $V_{\rm r} = \sqrt{\frac{\hbar\omega_{\rm r}}{L_{\rm r}c}}(b+b^\dagger)$ at the antinodes, where c is the transmission line capacitance per unit length, b ($b^\dagger$) is the annihilation (creation) operator associated with the photon. The quantized voltage $V_{\rm r}$ exerts on each CPB via a capacitance $C_{\rm r}^{(k)}$, and the coupling strength is

$$\lambda^{(k)} = \frac{eC_{\rm r}^{(k)}}{C_{\rm t}^{(k)}}\sqrt{\frac{\hbar\omega_{\rm r}}{L_{\rm r}c}}, \tag{18}$$

by which quantum state coupling between $|a\rangle^{(k)}|0\rangle$ and $|e\rangle^{(k)}|1\rangle$ can be induced through the creation and annihilation of microwave photons. According to Eq. (9), when $\lambda^{(k)}$ and $\Delta^{(k)}$ are fixed, the manipulations of $\Omega_{\rm eff}^{(k)}$ can be realized only by adjusting $\Omega_{\rm ag}^{(k)}$. For $\Phi_m^{(1)} \simeq 0.035\Phi_0\sin(\frac{3\pi}{2t_{\rm s}}t)$, the driving-induced coupling between $|a\rangle$ and $|g\rangle$ is $\Omega_{\rm ag}^{(1)}/2\pi \simeq -260\sin(\frac{3\pi}{2t_{\rm s}}t)$ MHz. With the given $\lambda^{(1)}/2\pi = 260$ MHz and $\Delta^{(1)}/2\pi = 2560$ MHz, there is $\Omega_{\rm eff}^{(1)}/2\pi \simeq 13.2\sin(\frac{3\pi}{2t_{\rm s}}t)$ MHz. For $\Phi_m^{(2)} \simeq 0.041\Phi_0\cos(\frac{3\pi}{2t_{\rm s}}t)$ and $\Phi_{\rm s}^{(2)} = 0.32\Phi_0$, we have $\Omega_{\rm ag}^{(2)}/2\pi \simeq -300\cos(\frac{3\pi}{2t_{\rm s}}t)$ MHz. In the case of $\Delta^{(2)}/2\pi = 3410$ MHz and $\lambda^{(2)}/2\pi = 300$ MHz, the effective Rabi coupling takes $\Omega_{\rm eff}^{(2)}/2\pi \simeq 13.2\cos(\frac{3\pi}{2t_{\rm s}}t)$ MHz. By a numerical simulation with the effective drivings, an initial state $|ge0\rangle$ can be fully transferred to $|eg0\rangle$ via the intermediate state $|ee1\rangle$, as exhibited in Fig. 4(c), where the SWAP gate needs a duration time $t_{\rm s} = 50$ ns for a selected $\varepsilon = \arcsin(3/4)$.

Physically, the quantum system of interest is unavoidably surrounded by noisy environment, leading to the qubit decoherence and cavity decay. By means of the standard dissipation theory, we now analyze the impact of decoherence effects on the gate operations. For the one-qubit gates, after tracing over the environmental degrees of freedom, we obtain the reduced density matrices ρ_x (with $x = n,\ p$), where $\rho_{n,p}$ are associated with the single-atom system of $\{|g\rangle, |a\rangle, |e\rangle\}^{(1)}$ and $\{|e\rangle, |f\rangle, |a\rangle\}^{(1)}$, respectively. In the Born–Markov approximation, the dynamical evolutions of ρ_x obey the Lindblad-type master equation

$$\frac{{\rm d}\rho_x}{{\rm d}t} = {\rm i}[\rho_x, H_x] + \sum_{j,l}^{j\neq l}\left\{\gamma^{(jl)}D[\sigma_-^{(jl)}]\rho_x + \frac{\gamma_\phi^{(jl)}}{2}D[\sigma_z^{(jl)}]\rho_x\right\}, \tag{19}$$

where the first term of the right side describes the decoherence-free evolution subject to H_x, and the other terms characterize the level relaxation and dephasing effects,[69] respectively. Here, $\gamma^{(jl)}$ ($\gamma_\phi^{(jl)}$) are the relaxation (dephasing) rates between states $|j\rangle$ and $|l\rangle$. The Lindblad superoperators are expressed as $D[L]\rho_x = (2L\rho_x L^\dagger - L^\dagger L\rho_x - \rho_x L^\dagger L)/2$, with $L = \sigma_-^{(jl)}$ and $\sigma_z^{(jl)}$. The inversion operators read $\sigma_-^{(jl)} = |l\rangle\langle j|$, and the Pauli operators are defined as $\sigma_z^{(jl)} = |j\rangle\langle j| - |l\rangle\langle l|$, in which the energy levels fulfill $E_j > E_l$. For the two-qubit gate, the time evolution of reduced density matrix $\rho_{\rm s}$ regarding $\{|ge0\rangle, |ee1\rangle, |eg0\rangle\}$ is governed by

$$\frac{{\rm d}\rho_{\rm s}}{{\rm d}t} = {\rm i}[\rho_{\rm s}, H_{\rm s}] + \kappa D[b]\rho_{\rm s}$$

$$+\sum_{k=1,2}\left\{\gamma^{(k)}D[\sigma_{-}^{(k)}]\rho_{\rm s}+\frac{\gamma_{\phi}^{(k)}}{2}D[\sigma_{z}^{(k)}]\rho_{\rm s}\right\}, \quad (20)$$

where κ indicates the decay rate of cavity photon, $\sigma_{-}^{(k)}=|g\rangle^{(k)}\langle e|$ is an inversion operator of the kth qubit, and $\sigma_{z}^{(k)}=|e\rangle^{(k)}\langle e|-|g\rangle^{(k)}\langle g|$.

To quantitatively represent the decoherence effects, we introduce the fidelities

$$F_{\rm g}=\left\langle\psi_i(t_{\rm g})\right|\rho(t_{\rm g})\left|\psi_i(t_{\rm g})\right\rangle, \quad (21)$$

where $F_{\rm g}$ (with $g=n$, p, and s) are the fidelities concerning NOT gate, phase gate, and SWAP gate, respectively; $\left|\psi_i(t_{\rm g})\right\rangle$ are ideal states at the final times $t=t_{\rm g}$, as displayed in Figs. 4(a), 4(b), and 4(c); and $\rho(t_{\rm g})=\left|\psi(t_{\rm g})\right\rangle\left\langle\psi(t_{\rm g})\right|$ denote the density matrices regarding the realistic states $\left|\psi(t_{\rm g})\right\rangle$. For simplicity, we choose $\gamma^{(jl)}=\gamma$ and $\gamma_{\phi}^{(jl)}=\gamma_{\phi}$ for the one-qubit gates, meanwhile, $\gamma^{(1)}=\gamma^{(2)}=\gamma$ and $\gamma_{\phi}^{(1)}=\gamma_{\phi}^{(2)}=\gamma_{\phi}$ for the two-qubit gate. By calculating Eqs. (19) and (21) with the accessible rates $\gamma/2\pi=0.02$ MHz and $\gamma_{\phi}/2\pi=0.1$ MHz,[27] we obtain $F_n=99.63\%$ and $F_{\rm p}=99.00\%$, respectively. The fidelity of two-qubit SWAP gate could reach up to $F_{\rm s}=96.72\%$ by numerically simulating Eqs. (20) and (21), where we have adopted a decay rate $\kappa/2\pi=0.25$ MHz.[70] These results imply that the shortcut-based approach can perform fault-tolerant operations, which can be mainly attributed to the shorter evolution times and inherent resilience to control parameter variations.

5. Discussions and conclusions

The proposed strategy may have the following advantages. (i) By suitably choosing the atom level spacings, the direct cross resonance that is caused by the cavity virtual excitations vanishingly exists between two artificial atoms, which is beneficial to mitigate error effect and then to enhance quantum robustness. (ii) The coupling between atoms inside a cavity field is flexibly switchable by manipulating the classical drivings. In this manner, we can implement one-qubit gate operations in a decoupled atom and a two-qubit SWAP gate in a composite qubit-photon-qubit system. The controllable qubit-qubit coupling contributes to explore quantum computing in a scalable multiqubit system. (ii) Compared with scheme mentioned in Ref. [71], the present two-qubit SWAP gate can be accomplished only in one step, which could provide a simplified way to experimental execution of the shortcut-based quantum gates.

In summary, we have developed an efficient protocol for constructing shortcuts to adiabatic quantum gates on superconducting qubits in circuit QED. Two artificial atoms of CPB circuits, having sufficient level anharmonicity, are placed in a common quantized cavity and are driven by individual classical microwaves. In a decoupled atom, a NOT gate and a π-phase gate can be constructed using the method of invariant-based shortcuts. With the assistance of cavity bus and by inversely engineering the Rabi drivings, a two-qubit SWAP gate only in one step can be acquired within a composite qubit-photon-qubit system. Moreover, we consider these gate implementations by virtue of the controllable microwave fields. Through numerically simulating the noise effects, it is found that the gates have high fidelities. The present strategy could offer a possibility of improving quantum computation with superconducting qubits.

References

[1] Steane A 1998 *Rep. Prog. Phys.* **61** 117
[2] Bennett C H and DiVincenzo D P 2000 *Nature* **404** 247
[3] Nielsen M A, Dowling M R, Gu M and Doherty A C 2006 *Science* **311** 1133
[4] Briegel H J, Browne D E, Dür W, Raussendorf R and Van den Nest M 2009 *Nat. Phys.* **5** 19
[5] Ladd T D, Jelezko F, Laflamme R, Nakamura Y, Monroe C and O'Brien J L 2010 *Nature* **464** 45
[6] Brandt H E 1999 *Prog. Quantum Electron.* **22** 257
[7] Zanardi P and Rasetti M 1999 *Phys. Lett. A* **264** 94
[8] Hicke C, Santos L F and Dykman M I 2006 *Phys. Rev. A* **73** 012342
[9] Chen Y H, Xia Y, Chen Q Q and Song J 2015 *Phys. Rev. A* **91** 012325
[10] Spiteri R J, Schmidt M, Ghosh J, Zahedinejad E and Sanders B C 2018 *New J. Phys.* **20** 113009
[11] Xu G F, Tong D M and Sjöqvist E 2018 *Phys. Rev. A* **98** 052315
[12] Dridi G, Mejatty M, Glaser S J and Sugny D 2020 *Phys. Rev. A* **101** 012321
[13] Zhou Z, Chu S I and Han S 2002 *Phys. Rev. B* **66** 054527
[14] Bladh K, Duty T, Gunnarsson D and Delsing P 2005 *New J. Phys.* **7** 180
[15] Pashkin Y A, Astafiev O, Yamamoto T, Nakamura Y and Tsai J S 2009 *Quantum Inf. Process.* **8** 55
[16] Liu W Y, Zheng D N and Zhao S P 2018 *Chin. Phys. B* **27** 027401
[17] Bækegaard T, Kristensen L B, Loft N J S, Andersen C K, Petrosyan D and Zinner N T 2019 *Sci. Rep.* **9** 13389
[18] Clarke J and Wilhelm F K 2008 *Nature* **453** 1031
[19] Devoret M H and Schoelkopf R J 2013 *Science* **339** 1169
[20] Wendin G 2017 *Rep. Prog. Phys.* **80** 106001
[21] Zhao S P, Liu Y X and Zheng D N 2018 *Acta Phys. Sin.* **67** 228501 (in Chinese)
[22] Guo Q *et al.* 2018 *Phys. Rev. Lett.* **121** 130501
[23] Yan R Y and Feng Z B 2020 *Adv. Quantum Technol.* **3** 2000088
[24] Blais A, Huang R S, Wallraff A, Girvin S M and Schoelkopf R J 2004 *Phys. Rev. A* **69** 062320
[25] Wallraff A *et al.* 2004 *Nature* **431** 162
[26] Billangeon P M, Tsai J S and Nakamura Y 2015 *Phys. Rev. B* **91** 094517
[27] Blais A *et al.* 2007 *Phys. Rev. A* **75** 032329
[28] Fedorov A, Steffen L, Baur M, da Silva M P and Wallraff A 2012 *Nature* **481** 170
[29] Abdumalikov Jr A A *et al.* 2013 *Nature* **496** 482
[30] Hua M, Tao M J and Deng F G 2015 *Sci. Rep.* **5** 9274
[31] Fan Y J, Zheng Z F, Zhang Y, Lu D M and Yang C P 2019 *Front. Phys.* **14** 21602
[32] Kang Y H and Xia Y 2020 *IEEE J. Sel. Top. Quantum Electron.* **26** 6700107
[33] Blais A, Girvin S M and Oliver W D 2020 *Nat. Phys.* **16** 247
[34] Chirolli L and Burkard G 2008 *Adv. Phys.* **57** 225
[35] Paladino E, Galperin Y M, Falci G and Altshuler B L 2014 *Rev. Mod. Phys.* **86** 361
[36] Montangero S, Calarco T and Fazio R 2007 *Phys. Rev. Lett.* **99** 170501
[37] Gladchenko S, Olaya D, Dupont-Ferrier E, Doucot B, Ioffe L B and Gershenson M E 2009 *Nat. Phys.* **5** 48
[38] Kamleitner I, Solinas P, Müller C, Shnirman A and Möttönen M 2011 *Phys. Rev. B* **83** 214518
[39] Dong D, Chen C, Qi B, Petersen I R and Nori F 2015 *Sci. Rep.* **5** 7873

[40] Wang Y, Zhang J, Wu C and You J Q and Romero G 2016 *Phys. Rev. A* **94** 012328
[41] Xue Z Y *et al.* 2017 *Phys. Rev. Appl.* **7** 054022
[42] Xu Y *et al.* 2018 *Phys. Rev. Lett.* **121** 110501
[43] Kang Y H, Chen Y H, Shi Z C, Huang B H, Song J and Xia Y 2019 *Ann. Phys. (Berlin)* **531** 1800427
[44] Bergmann K, Theuer H and Shore B W 1998 *Rev. Mod. Phys.* **70** 1003
[45] Bergmann K *et al.* 2019 *J. Phys. B: At. Mol. Opt. Phys.* **52** 202001
[46] Siewert J, Brandes T and Falci G 2009 *Phys. Rev. B* **79** 024504
[47] Feng Z B and Li M 2014 *Opt. Commun.* **319** 56
[48] Kumar K S, Vepsäläinen A, Danilin S and Paraoanu G S 2016 *Nat. Commun.* **7** 10628
[49] Torrontegui E *et al.* 2013 *Adv. At. Mol. Opt. Phys.* **62** 117
[50] Campo A and Kim K 2019 *New J. Phys.* **21** 050201
[51] Guéry-Odelin D, Ruschhaupt A, Kiely A, Torrontegui E, Martinez-Garaot S and Muga J G 2019 *Rev. Mod. Phys.* **91** 045001
[52] Yu L, Xu J, Wu J L and Ji X 2017 *Chin. Phys. B* **26** 060306
[53] Lu X J, Li M, Zhao Z Y, Zhang C L, Han H P, Feng Z B and Zhou Y Q 2017 *Phys. Rev. A* **96** 023843
[54] Chen Y H, Shi Z C, Song J, Xia Y and Zheng S B 2018 *Ann. Phys. (Berlin)* **530** 1700351
[55] Wang T *et al.* 2018 *New J. Phys.* **20** 065003
[56] Ma L H, Kang Y H, Shi Z C, Huang B H, Song J and Xia Y 2019 *Quantum Inf. Process.* **18** 65
[57] Yan T *et al.* 2019 *Phys. Rev. Lett.* **122** 080501
[58] Vepsäläinen A, Danilin S and Paraoanu G S 2019 *Sci. Adv.* **5** eaau5999
[59] Yu W R and Ji X 2019 *Acta Phys. Sin.* **68** 030302 (in Chinese)
[60] Yan R Y, Feng Z B, Li M, Zhang C L and Zhao Z Y 2020 *Ann. Phys. (Berlin)* **532** 1900613
[61] Yan R Y and Feng Z B 2021 *Opt. Laser Technol.* **135** 106699
[62] Vion D *et al.* 2002 *Science* **296** 886
[63] Majer J *et al.* 2007 *Nature* **449** 443
[64] Feng Z B 2012 *Phys. Rev. A* **85** 014302
[65] Feng Z B 2008 *Phys. Lett. A* **372** 3773
[66] Lewis H R and Riesenfeld W B 1969 *J. Math. Phys.* **10** 1458
[67] Liang Y, Wu Q C, Su S L, Ji X and Zhang S 2015 *Phys. Rev. A* **91** 032304
[68] Vitanov N V and Stenholm S 1997 *Phys. Rev. A* **55** 648
[69] Feng Z B, Lu X J, Li M, Yan R Y and Zhou Y Q 2007 *New J. Phys.* **19** 123023
[70] Schuster D I *et al.* 2007 *Nature* **445** 515
[71] Liang Y, Ji X, Wang H F and Zhang S 2015 *Laser Phys. Lett.* **12** 115201